Dimerization of the type IV pilin from *Pseudomonas aeruginosa* strain K122-4 results in increased helix stability as measured by time-resolved hydrogen-deuterium exchange

Cristina Lento,[1] Derek J. Wilson,[1,2,a)] and Gerald F. Audette[1,2,a)]
[1]*Department of Chemistry, York University, Toronto, Ontario M3J 1P3, Canada*
[2]*Centre for Research of Biomolecular Interactions, York University, Toronto, Ontario M3J 1P3, Canada*

(Received 3 March 2015; accepted 20 April 2015; published online 28 August 2015)

Truncated pilin monomers from *Pseudomonas aeruginosa* strain K122-4 (ΔK122) have been shown to enter a monomer-dimer equilibrium in solution prior to oligomerization into protein nanotubes. Here, we examine the structural changes occurring between the monomeric and dimeric states of ΔK122 using time-resolved hydrogen-deuterium exchange mass spectrometry. Based on levels of deuterium uptake, the N-terminal α-helix and the loop connecting the second and third strands of the anti-parallel *β*-sheet contribute significantly to pilin dimerization. Conversely, the antiparallel *β*-sheet and *αβ* loop region exhibit increased flexibility, while the receptor binding domain retains a rigid conformation in the equilibrium state.
[http://dx.doi.org/10.1063/1.4929597]

I. INTRODUCTION

Opportunistic infections by *Pseudomonas aeruginosa* are prevalent in patients with compromised immune systems including those recovering from burn wounds[1–3] and organ transplants,[4,5] as well as in individuals suffering from cystic fibrosis,[6,7] acute leukemia,[8] and HIV.[9] These persistent infections are initiated by interaction of a type IV pilus (T4P) with receptors on the mucosal cells of susceptible hosts.[10–15] T4P are also responsible for a variety of bacterial processes including surface motility,[14,16–19] microcolony and biofilm formation,[14,20–23] cell-host adhesion,[15] cell signalling,[24] and DNA uptake.[25,26] Indeed, T4P are important structures found across a wide range of gram-negative and gram-positive bacteria, and disruption of the pilus leads to decreased bacterial virulence in many gram-negative pathogens.[2,13,14,27,28]

The type IV pilus is a filamentous protein polymer of single monomeric unit, the type 4 pilin. Based on sequence similarities/differences in the pilin protein, there are two main pili sub-types: the IVa (T4aP) and IVb (T4bP) pili.[14] The T4b pilins are a heterogeneous group common in enteric species such as *V. cholerae* and *S. typhi*, whereas T4a pilins, including those observed in *P. aeruginosa*, are more broadly distributed.[14] Structurally, the type IV pilin (*pilA*) monomer is comprised of an α-helix connected by a variable *αβ*-loop to a four-stranded antiparallel *β*-sheet; surface and cellular adherence are mediated through a conserved C-terminal loop known as the D-region (Figure 1(a)).[29–38] In the *P. aeruginosa* pilins, the N-terminal region of the α-helix (α1-N) is both highly conserved and hydrophobic, whereas the C-terminal region of the helix (α1-C) is amphipathic and packs onto the *β*-sheet.[30–33] The pilins are assembled/disassembled by a membrane-spanning complex whose architecture is evolutionarily related to a type II secretion system[14,16,39] into a pilus several microns in length with an approximate outer

a)Authors to whom correspondence should be addressed. Electronic addresses: dkwilson@yorku.ca and audette@yorku.ca

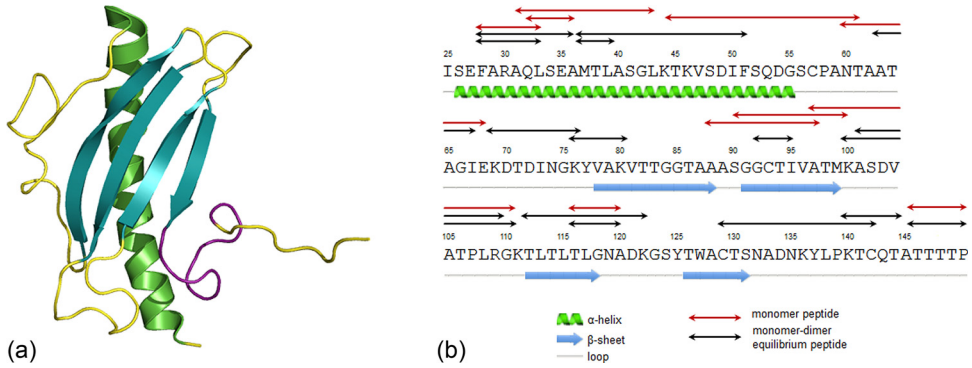

FIG. 1. Structural elements of the ΔK122 pilin, and the peptides analyzed in this study. (a) The common structural features of type IV pilins are highlighted on the ΔK122 monomer: the four-stranded antiparallel β-sheet (cyan), the truncated N-terminal α-helix (green), connecting loop regions (yellow), and the receptor binding D-region (purple). (b) The secondary sequence is numbered taking into account the truncated portion of the α-helix. The peptic peptides obtained in this study are highlighted using red and black double ended arrows. Figures 1(a), 4(b), 5(a), and 6(b) were produced with Pymol[63] using the 1.54 Å resolution structure (PDB ID 1QVE) of the ΔK122 pilin.[32]

diameter of 6–8 nm.[14–16,37,40–43] Cryo-electron microscopy[36,37,44] and fibre diffraction[45] studies of *P. aeruginosa* T4P have shown that assembly is through a three-start helical assembly of pilin monomers to the base of the pilus.[15,41,44]

From a bionanotechnology perspective, T4P form robust nanofibers with the ability to bind biotic and abiotic surfaces via their tips, interactions which have been mapped to the D-region of the pilin.[12] It has been estimated that the attractive force between the native T4P tip and steel is in excess of 100 pN/molecular interaction[46] and for *in vitro* derived D-region peptides and protein nanotubes is in the range of 26–55 and 78–165 pN/molecular interaction, respectively.[47,48] Functional nanostructures have been generated from native bacterial pili and explored for their potential use as biological nanowires. The development of protein-based nanofibers and nanotubes has several advantages when compared to their inorganic counterparts such as carbon nanotubes, which are significantly more cytotoxic and pose compatibility issues. Studies have shown that cultures of *Geobacter sulfurreducens* produce biofilms with one of the highest known current densities in microbial-based fuel cells[49,50] and are capable of long-range metallic-like conductivity[51] and supercapacitor behaviour[52] through a T4P network. These properties make microbial biofilms and T4P exciting prospects for use as a low cost and environmentally sustainable form of energy storage. Additionally, the β-sheet and connecting loops that form the surface of T4P show extremely high sequence variability, which allows for the use of protein engineering strategies to design fibers with altered surface characteristics. Also, if we consider binding of T4P to biotic surfaces such as epithelial cells, this opens an exciting area for further research in therapeutics. As is the case with binding to abiotic surfaces, the D-region of the pilin is responsible for forming specific interactions with cellular glycolipids.[47] This receptor-specific interaction could allow for targeted drug delivery of the therapeutic-loaded T4P-based nanocarriers.

While there are several structural studies of pilins and T4P, the end points of assembly, structural studies of the initial to intermediate stages of pilus assembly have been more challenging. Current T4P models[15,37,41,44] place the α-helix within the interior of the fibril; T4P formation is driven by the hydrophobic α1-N region of the helix, and the β-sheet of the globular head domain defines the outer face of the pilus. The $\alpha\beta$-loop of the pilin is predicted to interact with neighbouring subunits due to its size and position with respect to the globular domain,[15,41,44] while the D-region is predicted to be occluded and only exposed at the tip in order to bind receptors on epithelial cells.[12] Recently, a truncated form of the pilin from *P. aeruginosa* strain K122-4 (ΔK122) lacking the conserved α1-N region of the helix has been shown to form T4P-like structures, so called protein nanotubes (PNTs), both in solution and at surfaces.[48,53–55] As this truncated form of the pilin lacks the predicted main driving force for pilus oligomerization, namely the conserved α1-N region, other protein-protein interactions are required to stabilize the

structure during the oligomerization process. It has also been observed that the ΔK122 pilin forms a monomer-dimer equilibrium in solution prior to fibril and PNT oligomerization.[55]

In the current study, we employ Time-Resolved ElectroSpray Ionization Hydrogen-Deuterium eXchange (TRESI-HDX) mass spectrometry, which allows for kinetic experiments to be carried out with reaction times ranging from milliseconds to seconds,[56,57] to study the dynamics of the ΔK122 pilin. Incorporation of a kinetic mixer onto a microfluidic chip in combination with hydrogen-deuterium exchange (HDX) studies facilitates an analysis of the local dynamics of proteins undergoing biologically relevant conformational transitions. To achieve these measurements, the protein is incubated with deuterium at sub-second time scales and then enters a proteolysis microreactor which is held at low pH in order to quench the exchange reaction. Amide hydrogen atoms on the protein backbone function as exchangeable reporters and allow for the mapping of protein-protein interaction interfaces and identification of localized areas undergoing structural change.[58] Our TRESI-HDX mass spectrometry experiments provide insights on the changes in structural dynamics of the protein in the monomer-dimer equilibrium and compare them to the protein in the monomeric state in order to map the interfaces that are involved in the dimerization. Understanding the structural changes that occur in this equilibrium state will shed light on the earliest intermediate leading up to fibril formation and PNT oligomerization.

II. EXPERIMENT

A. Chemicals and supplies

All chemicals were purchased from Sigma-Aldrich, Thermo Fisher Scientific, or BioBasic, and were of ACS grade or higher. Ultrapure water was generated in-house on a Millipore Milli-Q Advantage A10 system. All liquid chromatography was carried out using the ÄKTA Purifier 10 (GE Healthcare), with amylose resin purchased from New England Biolabs, and ion exchange resin (Source 30S) purchased from GE Healthcare. Pepsin agarose beads, deuterium oxide (D_2O), ammonium acetate, and acetic acid were purchased from Sigma-Aldrich.

B. Expression and purification of the ΔK122 pilin

The truncated form of the monomeric type IV pilin from *P. aeruginosa* strain K122-4 [*pilA* (Δ1-28); ΔK122] was expressed and purified as previously reported.[32,55] Briefly, *Escherichia coli* strain ER2507 cells harbouring the pMAL-p2X vector encoding MBP-ΔK122 were cultured overnight at 37 °C with shaking in Luria-Bertani (LB) medium containing 50 μg/ml ampicillin, which was then used as seed stock for a day culture that was grown in LB containing 50 μg/ml ampicillin and 10 mM glucose until mid-log phase was reached (OD_{600} 0.5–0.7). Protein expression was induced at 30 °C with shaking at 200 rpm using IPTG at a final concentration of 1 mM for 4 h. The induced cells were harvested by centrifugation at 6000 × g for 20 min at 4 °C. MBP-ΔK122 was released from pelleted cells using an osmotic shock method.[59] Cell pellets were resuspended in 10 mM tris(hydroxymethyl)aminomethane (tris, pH = 7.4) and 20% sucrose and incubated on ice for 25 min with gentle shaking. The cells were then centrifuged at 7000 × g for 20 min at 4 °C. The supernatant was removed and the pellet resuspended in 5 mM magnesium sulphate ($MgSO_4$) and incubated on ice for 25 min with gentle shaking, following which the cells were centrifuged at 35 000 × g for 20 min at 4 °C. The supernatant was syringe filtered using a 0.45 μm membrane and MBP-ΔK122 was isolated by affinity chromatography.

The periplasmic solution containing MBP-ΔK122 was loaded onto amylose beads equilibrated with 20 mM tris-HCl pH 7.4, 200 mM NaCl and 1 mM EDTA. Following washing the column with several column volumes of loading buffer, MBP-ΔK122 was eluted from the column with an elution buffer containing 20 mM tris-HCl pH 7.4, 10 mM maltose, and 1 mM EDTA. The ΔK122 protein was then released from the MBP affinity tag through tryptic digestion where the fusion protein was incubated on ice for 10 min at a 1:500 v/v ratio of trypsin to protein ratio. Proteolysis was quenched by the addition of phenylmethylsulfonyl fluoride (PMSF) protease inhibitor at a 10:1 v/v ratio of PMSF to trypsin. ΔK122 was purified from the

digestion mixture by cation exchange chromatography (CIEX) on a column equilibrated with 10 mM tris-HCl pH 7.4 using a linear 0–1 M NaCl gradient. Protein containing fractions were analyzed using 12.5% sodium dodecyl sulfate polyacrylamide gel electrophoresis (SDS-PAGE). Native PAGE was used to confirm the presence of a monomer-dimer equilibrium immediately after purification. The protein was then concentrated and buffer exchanged into 50 mM ammonium acetate using a dialysis cassette prior to analysis by mass spectrometry.

C. Electrospray ionization—ion-mobility spectrometry—mass spectrometry (ESI-IMS-MS)

ΔK122 concentrated to 10 μM in 50 mM ammonium acetate was infused into a Waters Synapt G1 Mass Spectrometer and readings were taken within the 2400–5000 m/z range. The protein was infused at a flow rate of 2 μl/min with the capillary voltage set at 2.5 kV, the sampling cone at 200 V, extraction cone at 2.0 V, and backing pressure set to 4.56 mbar.

D. Microfluidic device fabrication

The microfluidic device was made on a blank poly(methyl methacrylate) (PMMA) substrate purchased from Professional Plastics (Fullerton, CA) measuring 8.9 cm × 3.8 cm × 0.6 cm. The microfluidic channels outlining the protein channel, two acid channels, and the pepsin reaction chamber was etched onto the PMMA chip by laser ablation using a *Versa*Laser™ laser engraver (Universal Laser, Scottsdale, AZ). The microfluidic channel design was generated in CorelDraw X3 (Corel, Ottawa, ON) as previously described.[60] A 28RW sized metal capillary was incorporated into the central channel of the device using a soldering iron. Two additional 27RW sized metal capillaries for acid delivery were incorporated in similar fashion on both sides of the central channel. A mobile polyimide coated glass capillary with an outer diameter (o.d.) of 153 μm was inserted into the central 28RW metal capillary onto which a 2 mm notch was made. A deuterium oxide (D_2O) channel was connected to the central capillary via a T-junction (Figure 2). Polyimide coated glass capillaries (o.d. 153 μm, i.d. 75 μm) were supplied by Polymicro Technologies (Phoenix, AZ). Metal capillaries (28RW, 27RW) were supplied by McMaster-Carr (Aurora, OH).

E. Hydrogen-deuterium exchange

Following microfluidic chip construction, pepsin agarose beads were inserted into the proteolytic chamber and activated using hydrochloric acid (pH 1.8) for 1 h followed by acetic acid (pH 2.3) for 1 h. Silicone rubber cut with an outline of the reaction well was placed between the fabricated PMMA chip and a blank chip to generate a liquid-tight seal between the two PMMA blocks. The sandwich was then placed in a metal clamp (LAC Machine & Tooling Limited, ON) to pressure-seal the microfluidic device. All acid, protein, and deuterium channels were connected to Harvard 11 + infusion syringe pumps (Holliston, MA) to administer respective flow rates. Freshly prepared protein was passed through the inner glass capillary, exits through the notch, and becomes deuterated. Moving the inner glass capillary backwards within the central channel changes the reaction volume and allows one to track a reaction through various time points between mixing and ESI. In this study, labelling times ranging from 200 to 2000 ms were acquired.

F. Data analysis

Time-resolved hydrogen deuterium exchange mass spectrometry was carried out on a Q-Star Elite quadrupole time-of-flight (Q-TOF) instrument (MDS Analytical Technologies, Concord, ON). The instrument was operated in positive ion mode with a source voltage of 2600 V. All data were acquired at a rate of 1 s^{-1} and the samples were scanned over the 350–2000 m/z range. The resulting peptic digest of ΔK122 was analyzed using FindPept tool on the ExPASy Proteomics server (Swiss Institute of Bioinformatics, Basel), allowing for site-specific localization of uptake values. The peptides obtained for the monomer and equilibrium state are

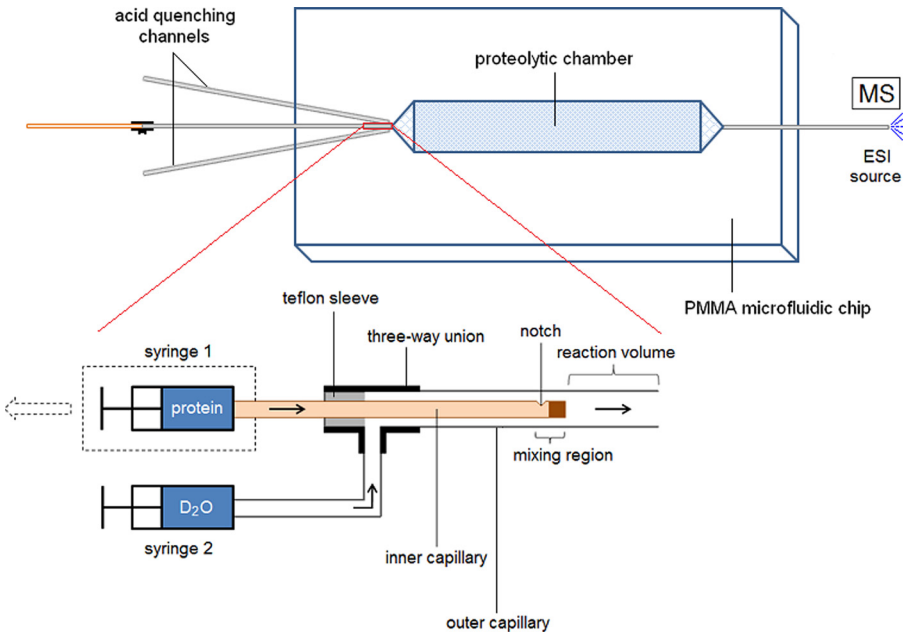

FIG. 2. Experimental setup for time-resolved HDX-MS. The kinetic mixer is integrated into a microfluidic chip along with acid quenching channels and a downstream proteolytic chamber containing pepsin agarose beads. The distal capillary is used as an ESI source. A zoomed in view of the kinetic mixer with adjustable reaction volume is also shown. Two concentric capillaries are injected with reactants from syringe 1 (containing protein) and syringe 2 (containing deuterium). A notch is made 2 mm from the end of the inner capillary and plugged at the end allowing for protein to exit from the inner capillary and efficiently mix with the incoming deuterium. Changing the position of the inner capillary within the outer capillary changes the volume between mixing and ESI detection allowing for the continuous tracking of the reaction over various time points.

highlighted in Figure 1(b). The experimental deuterium uptake of each peptide obtained was calculated using in-house developed FORTRAN software (D.J.W., unpublished results). In parallel, the intrinsic rates of each peptide were calculated using SPHERE (http://www.fccc.edu/research/labs/roder/sphere/).[61] The observed experimental and intrinsic uptake values were plotted as a function of reaction time and fit to single exponential expressions in Sigma Plot 11.0. Error bars represent standard deviation values where at least 3 replicate runs were obtained. Due to the nature of the method and low sequence specificity of pepsin cleavage, low intensity peptides are sometimes lost during some intervals of the experiment and thus only 1 or 2 data points were obtained.

III. RESULTS AND DISCUSSION

A previous study by Petrov and colleagues showed that following removal of the MBP fusion partner, ΔK122 exists in a monomer-dimer equilibrium in solution and that upon incubation with 2-methyl-2,4-pentanediol (MPD), high molecular weight oligomers (fibrils and PNTs) are formed.[55] This monomer-dimer equilibrium can be observed in a native PAGE gel, which shows two distinct bands at approximately 13 and 26 kDa after cation exchange purification to separate ΔK122 from the MBP (Figure 3(a)). Analysis of the purified protein using native ESI-IMS-MS shows two conformations present at the +4 monomeric charge state corresponding to an m/z charge of 3210, as well as low-abundance species at m/z 2869 and 3669, which correspond to ΔK122 dimers with odd charge states (Figure 3(b)).

The observation that the MBP tag facilitates the maintenance of the ΔK122 pilin as a monomer, and removal of the MBP results in ΔK122 entering into a monomer-dimer equilibrium (Figure 3(a)) is advantageous for the characterization of each state via hydrogen-deuterium exchange. The MBP-ΔK122 fusion acts as the "time 0" monomer, while analysis of ΔK122 following removal of MBP provides details on the monomer-dimer equilibrium.

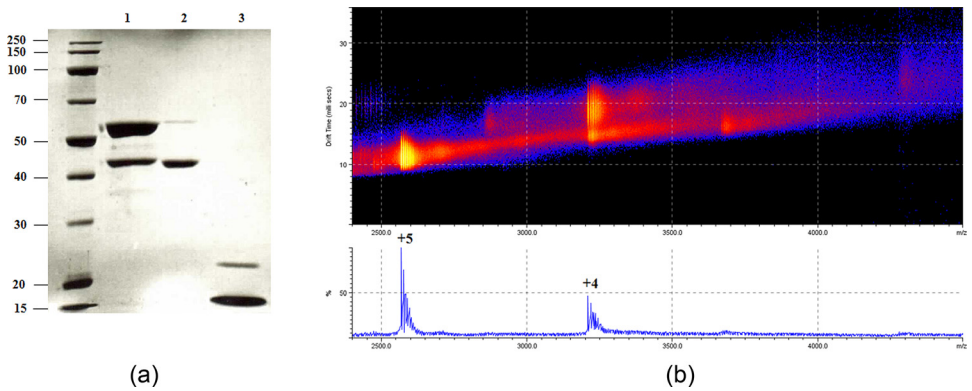

FIG. 3. Observance of a ΔK122 monomer-dimer equilibrium. (a) Native PAGE analysis of ΔK122 following cation exchange purification. Lane 1 is the eluted peak from the amylose resin purification showing the presence of MBP-ΔK122 (upper band) and free MBP (lower band); lane 2 is the flow through of the cation exchange purification (MBP and residual MBP-ΔK122); lane 3 is the purified ΔK122 (100 μM) showing the presence of a monomer (13 kDa) and dimer (26 kDa) equilibrium in solution; molecular weight markers are in the left most lane. (b) Observance of the monomer-dimer equilibrium by ESI-IMS-MS via a 3D Driftscope plot (m/z vs. drift time vs. intensity). Monomer peaks corresponding to the +5 ($m/z = 2568$) and +4 ($m/z = 3210$) charge states are predominant. In addition, there are faint dimer peaks present in between the monomer peaks in the spectrum as well as ion mobility plot.

Analysis of the digested MBP-ΔK122 fusion protein proved challenging due to spectral overlap of peptides originating from the large MBP tag. Despite these challenges, a 59% sequence coverage of the ΔK122 pilin was achieved (Figure 4(b)). Segments are color-coded by deuterium uptake at the final time point obtained, corresponding to a labelling time of 2000 ms. The N-terminal region of the amphipathic α-helix, in particular, the peptide FARAQLSEA (a.a. 28–36), shows high dynamic flexibility; this peptide is close to Gly42 (Figure 1), which induces a kink in the helix due to its increased stereochemical flexibility.[32] The observed dynamic flexibility of this peptide is consistent with NMR data for the ΔK122 pilin ($\Delta K122^{NMR}$),[31] which showed that the N-terminal end of the α1-C helix is deflected away from the β-sheet. Accordingly, a comparison of $\Delta K122^{NMR}$ and crystallographically determined structures of the protein[32] reveals that an otherwise conserved hydrogen bond between the side chain O^{ε} of Gln 32 and the amide nitrogen of Ala 105 is missing. This could partially account for the observed high exchange rate as the helix is afforded more relative motion from the β-sheet and has less local i + 4 hydrogen bond stability. These data suggest that the packing of the hydrophobic core in ΔK122, specifically the N-terminal end of the helix, is less tight thereby allowing for

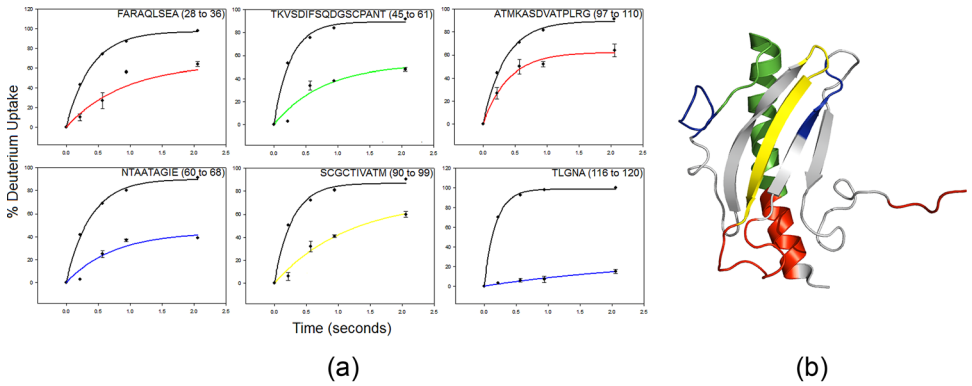

FIG. 4. HDX analysis of the ΔK122 monomer. (a) Representative kinetic plots of % deuterium uptake vs. time for 6 peptides from ΔK122. The intrinsic rate of the peptide is shown in black while the experimental uptake is shown in colour. Error bars represent standard deviation values where 3 or more replicates were obtained. (b) Differing levels of deuterium uptake for the monomer were mapped onto the structure of ΔK122. The measured profiles are coloured according to total deuterium uptake: red (61%–100%), yellow (51%–60%), green (41%–50%), and blue (0%–40%); regions for which no peptides were observed are coloured in grey.

structural flexibility. In contrast, the C-terminal region of the helix exhibits relatively low deuterium uptake, suggesting that this end of the helix exhibits more stable hydrogen bonding and is more tightly packed alongside one or more strands of the β-sheet.

The connecting loop between the second and third strands of the antiparallel β-sheet also exhibits some of the highest exchange rates in the monomer, which is not surprising due to the lack of a stabilizing H-bonding network between structural elements. The second strand of the sheet shows moderate-to-high deuterium uptake throughout. The moderate-to-high uptake may be a the result of the α-helix lying at a 45° angle relative to the surface of the β-sheet, as observed in $\Delta K122^{NMR}$,[31] allowing for more overall solvent exposure in parts of the network. The low level of exchange for the NTAATAGIE peptide (a.a. 60–68) located within the $\alpha\beta$-loop was unexpected and suggests that it is tightly packed in the monomeric state forming a loop-protein packing interface. Finally, the C-terminal end of the protein shows complete deuterium uptake, which is consistent with NMR observations[31] suggesting that this region of the protein is highly mobile in solution. Representative kinetic plots for the monomeric peptides are shown in Figure 4.

Following removal of the MBP tag, ΔK122 enters a monomer-dimer equilibrium; TRESI-HDX analysis of the protein results in a sequence coverage of 73% (Figure 5). Examination of the relative deuterium uptake levels of the protein in this state can provide insight on the changes in dynamic flexibility, solvent exposure, and the domains likely involved in protein-protein interactions. Representative spectra of peptides obtained over the time course of the reaction exhibiting shifts in isotopic distribution upon exposure to deuterium are shown (Figure 5(b)). The amphipathic α-helix (the α1-C region of the protein) shows a considerable decrease in deuterium uptake compared to the monomer. Indeed, the FARAQLSEA (a.a. 28–36) peptide shows a decrease from 64% $\pm$ 2.29 to 49% $\pm$ 4.50, and the region spanning ASGLKTKVSDIF (a.a. 40–51) shows a decrease from 48% $\pm$ 1.52 to 32% $\pm$ 2.12. These data suggest that stabilization of the truncated monomer is a result of interaction along the α-helix. Interestingly, the connecting loop region spanning KASDVATPLRG (a.a. 100–110) also shows a significant decrease in uptake, suggesting that it is either directly involved in protein-protein interaction within the dimer or serves to stabilize the interaction.

In the equilibrium state, the antiparallel β-sheet network shows variable exchange rates ranging from low to high deuterium uptake. In particular, the GCTI (a.a. 92–95) and TLGNA (a.a. 116–120) peptides exhibit increased uptake in the monomer-dimer equilibrium. This may be the result of destabilization of the hydrogen bonding network as the α-helix involved in protein-protein interactions moves away from the β-sheet. It is possible that the truncated helix shifts outward in order to form the interaction required for dimerization prior to fibril assembly. This is consistent with NMR data of the pilin,[31] which shows that the α-helix is less tightly packed on the β-sheet prior to oligomerization. In addition, the ATAGI (63–67) peptide within the $\alpha\beta$-loop shows high uptake relative to the monomer, indicating a state of increased dynamic flexibility. This could be the result of the loop having to move away in order to accommodate the incoming protein for dimerization. Representative kinetic plots of deuterium uptake over time for the peptides showing either a decrease or increase relative to the monomer are shown (Figure 5(c)).

One of the regions that was not analyzed in the monomeric protein but appears for the equilibrium state is the disulfide bonded receptor binding domain, or D-region. The D-region consists of a type I followed by a type II turn forming a V-shaped groove whose side chains protrude toward the protein interior, in particular, toward the α1-C helix, stabilizing the double-turn conformation.[30,32] Accordingly, the peptide CTSNADNKYLPKTC (a.a. 129–142), which falls within the D-region, displays some of the lowest uptake levels of the protein. This indicates that the backbone amide hydrogens are hidden from the solvent and point up into the pocket, which correlates with crystallographic observations of ΔK122.[32] It is interesting to note that of the seven conserved residues in the globular domain of pilins originating from *Pseudomonas* three are located within the D-region, Cys 129 and Cys 142, which form a disulfide bridge that bounds the D-region, and Pro 139, which initiates the second β-turn of this region.[26,30,32] It is therefore not surprising that the disulfide bond and proline residue would

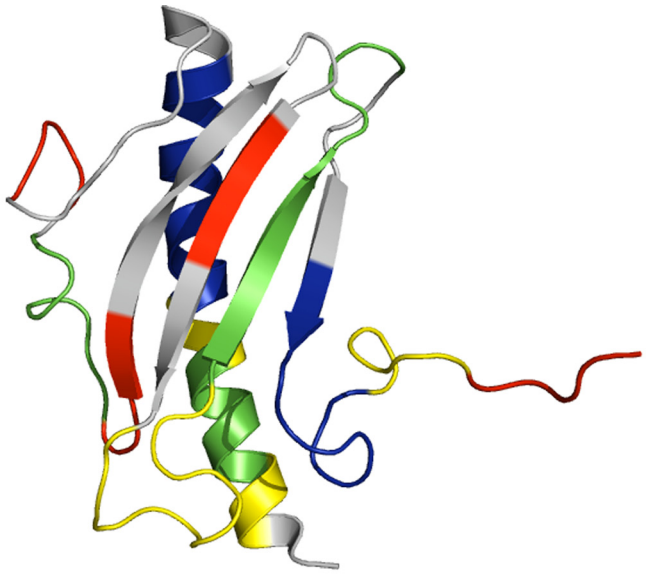

(a)

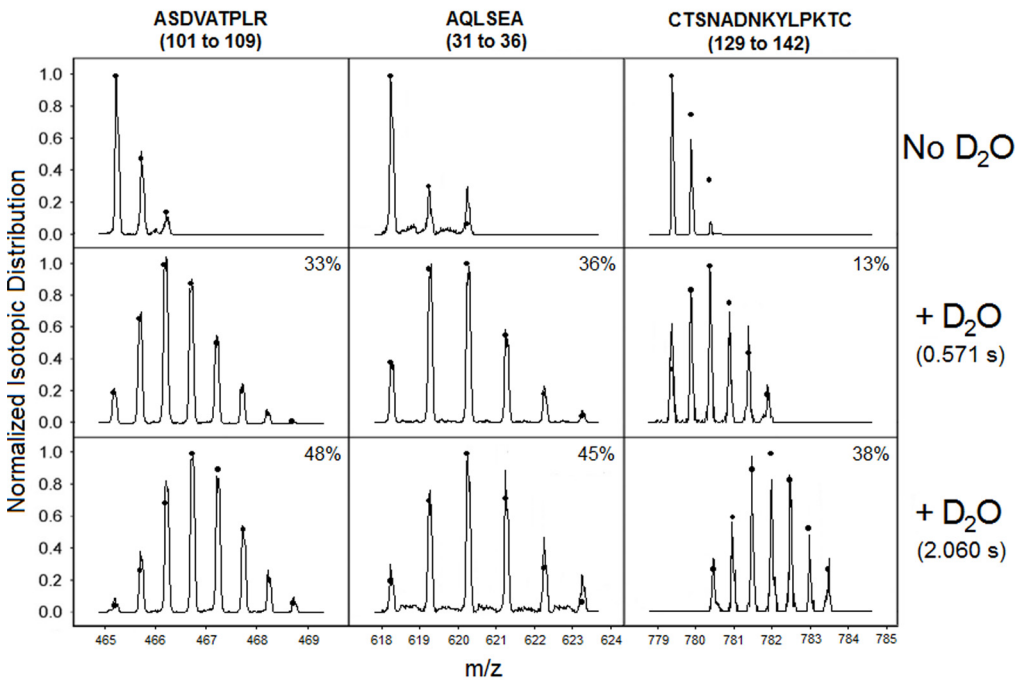

(b)

FIG. 5. HDX analysis of the ΔK122 monomer-dimer equilibrium. (a) Differing levels of deuterium uptake for the monomer-dimer equilibrium mapped onto the solution structure of ΔK122. The measured profiles are coloured according to total deuterium uptake: red (61%–100%), yellow (51%–60%), green (41%–50%), and blue (0%–40%); regions for which no peptides were observed are coloured in grey. (b) Site-specific HDX analysis for the equilibrium state. Representative spectra of peptides for non-deuterated ΔK122 (top panel) and upon incubation with deuterium at 0.571 s and 2.060 s. Raw spectra exhibit shifts in isotopic distribution upon exposure to deuterium. Percent deuterium uptake is indicated on each spectrum. (c) Representative kinetic plots of % deuterium uptake vs. time for 6 peptides from ΔK122. The intrinsic rate of the peptide is shown in black, while the experimental uptake is shown in colour. The top three panels represent peptides that show a decrease in deuterium uptake in the monomer-dimer equilibrium, while the bottom three panels represent peptides that show an increase in deuterium uptake. Error bars represent standard deviation values where 3 or more replicates were obtained.

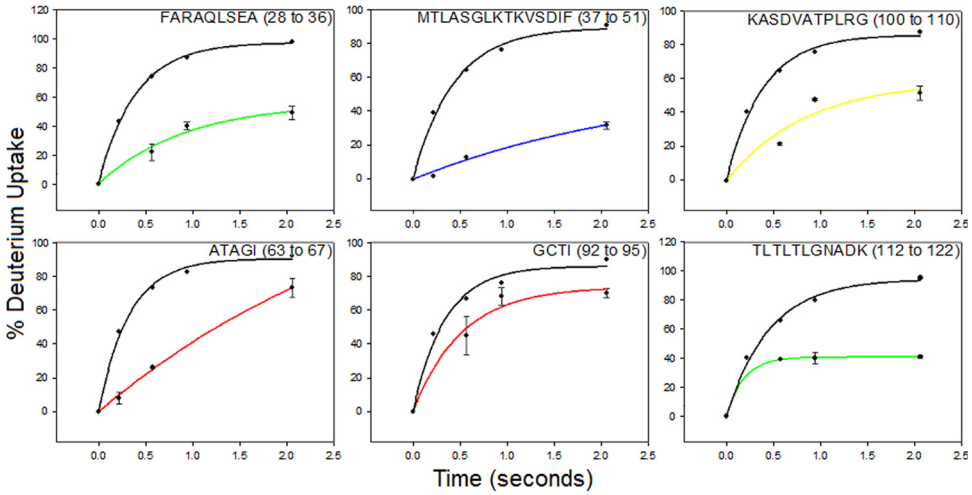

(c)

FIG. 5. (*Continued*)

increase the rigidity of this region as they restrict conformational flexibility. In previously solved pilin structures, the side chains of the cysteine and proline residues are buried towards the core of the protein, defining a packing interface.[32] This agrees with previous NMR data showing that the disulfide loop exhibits a rigid backbone conformation essential for attachment to host cell receptors.[62] In addition, interactions between the $\alpha\beta$-loop and D-region have been proposed for the K122-4 pilus based on the charge complementarity in these regions.[13,31,37,41,44] Following the D-region is the disordered C-terminal loop which continues to show high deuterium uptake at equilibrium, albeit slightly lower compared to it being fully saturated in the monomer.

The use of pilin-derived PNTs for biomedical applications is attractive due to their well-defined structures, assembly under physiologically relevant conditions, and easy manipulation through protein engineering approaches. However, in order to fully exploit these structures, an understanding of their assembly from monomer (pilin) to polymer (pilus) is required. Currently, there are structural models for the monomer (the pilin)[29–38] and the polymer (the pilus),[14,16,36,37,40,45] and the generation of the T4P from the monomeric pilin by the bacterium is reasonably well understood.[14–16,39,41,43,44] On the other hand, the truncated ΔK122 pilin does not have (a) the bacterial machinery to guide assembly nor (b) the hydrophobic N-terminal region of the α-helix to hydrophobically drive pilin oligomerization into PNTs. An experimentally derived structure of a full length pilin-derived PNT remains elusive, and the mechanism of oligomerization is less well understood, although it has been shown that it follows a fibril-mediated process.[55] Our observation that the pilin enters a monomer-dimer equilibrium upon purification away from its MBP fusion partner (Figure 3) allowed us to explore a very early time point in the oligomerization process. It was not fully unexpected to observe the rigidity of the receptor binding D-region (Figure 5), especially noting that this region is structurally maintained for receptor binding despite sequence diversity among the *P. aeruginosa* pilins.[32] The observation that peptides from the N-terminal region of the α-helix, in particular, the FARAQLSEA (a.a. 28–36) peptide, show a decrease in deuterium uptake and therefore reduced flexibility, indicates that while the full helix is not present, this portion of the helix plays an important role in the early points of pilin fibril formation. In addition, the increased stability of the loop connecting the second and third strands of the anti-parallel β-sheet suggests that it also plays a role in dimerization of the pilin, perhaps through increased interaction with the N-terminal region of the α-helix (Figure 6). Also, the increased flexibility observed in the $\alpha\beta$-loop region may be a result of a structural requirement induced by the altered packing of the α-helix onto the β-sheet in the dimer, resulting in the occlusion of the D-region in the PNT structure.

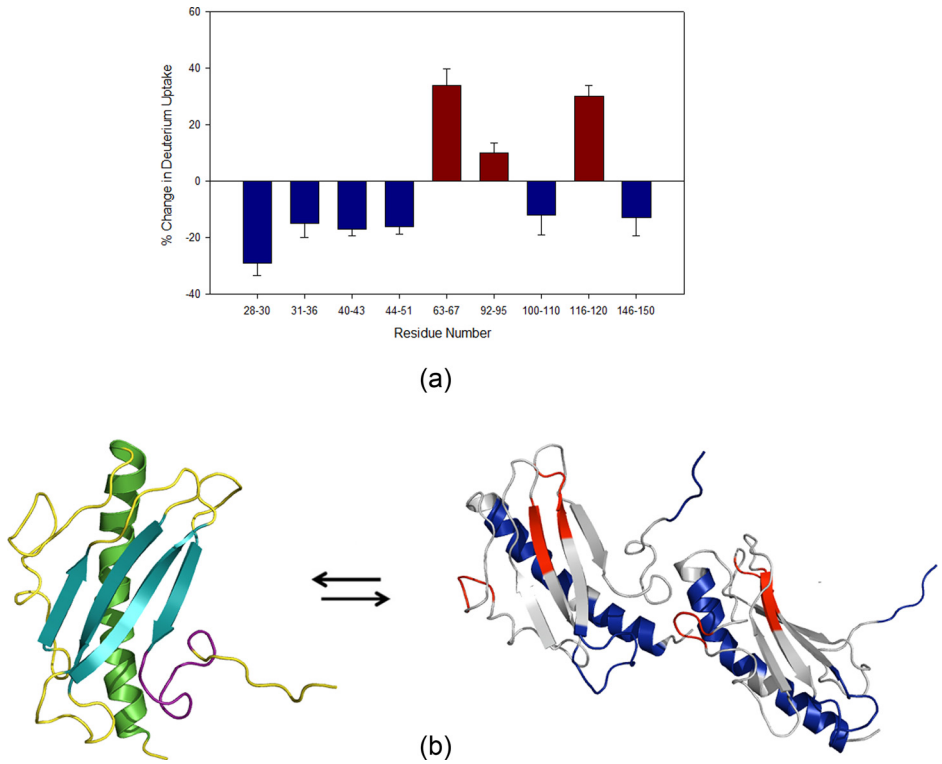

FIG. 6. Localization of the changes that occurs in the monomer-dimer equilibrium. (a) Significant differences in the relative deuterium uptake in overlapping stretches of the protein are shown, with error bars representing the standard deviation of 3 or more replicates. (b) The structural elements of the monomer are coloured as described in Figure 1. In the dimer (right), peptides coloured in blue represent a significant decrease in uptake for the equilibrium state, and those in red represent a significant increase in uptake. Based on changes in hydrogen-deuterium exchange, interactions occur between the amphipathic α-helix in the dimer, as well as possible involvement of a connecting loop. The truncated helix shifts further outward in order to form the interaction required for dimerization, destabilizing the β-sheet network. The model of the dimer was generated using a 3-start helical assembly model for the T4P.[44]

Together, these observations point to regions of the pilin that may be useful to exploit in terms of varying oligomerization kinetics and or fibril/PNT stability; research is on-going to further characterize the structural and mechanistic requirements of pilin-derived PNT oligomerization and to develop these structures for biomedical applications.

IV. CONCLUSION

In the current study, we analyzed the dynamics the ΔK122 pilin protein, both in the monomeric state (as a MBP-ΔK122 fusion protein) and in the pre-fibrillar dimer state at the millisecond time scale using TRESI-HDX-MS. A summary of the regions showing significant increases and decreases between the two states is mapped onto the protein sequence (Figure 6(a)). Results point toward the site of protein interaction mainly occurring along the amphipathic α-helix as well as possible involvement of a connecting loop. This is consistent with the α-helix having high sequence conservation among the pilins (for instance in *P. aeruginosa* strains K122-4, PAK, PAO, and *Neisseria gonorrhoeae* strain MS-11).[31] In addition, variable exchange rates ranging from moderate to high in the β-sheet network and $\alpha\beta$-loop indicate that these regions show increased dynamic flexibility in the dimer. Finally, the D-region responsible for receptor binding shows low deuterium uptake in the monomer-dimer equilibrium and suggests both structural rigidity and solvent protection. Overall, the results indicate that the truncated α-helix shifts in order to increase helix-helix interactions in the dimer, imparting stabilization of the dimeric precursor prior to coalescence into protein fibrils. The proposed interaction mechanism of dimerization (Figure 6(b)) results in a stabilization of the α-helix through the

protein-protein interaction interface. Movement of the helix away from the β-sheet network might account for the destabilization seen in peptides falling within this region.

Understanding the structural changes that occur when the protein enters its dimeric state is of great importance as it is the earliest intermediate leading up to protein nanotube formation. Stabilization of the pilin dimer should result in more rapid fibril formation and PNT oligomerization. Characterization of the structural changes that occur during the formation of pilin-derived PNTs can also provide a greater understanding behind the mechanism of T4P formation as well as allowing for the development of these structures for applications in bionanotechnology. Efforts are on-going in understanding how the pilin oligomerizes from this equilibrium state to higher molecular weight species forming protein-derived nanofibrils and eventually PNTs.

ACKNOWLEDGMENTS

This research was supported by grants from the Natural Sciences & Engineering Council of Canada (NSERC), the Canadian Foundation for Innovation (CFI) and York University. C.L. gratefully acknowledges financial support from the Ontario Graduate Scholarship program, NSERC and York University.

[1]B. A. Pruitt, Jr., A. T. McManus, S. H. Kim, and C. W. Goodwin, "Burn wound infections: current status," World J. Surg. **22**(2), 135–145 (1998).
[2]L. C. D'Avignon, B. K. Hogan, C. K. Murray, F. L. Loo, D. R. Hospenthal, L. C. Cancio, S. H. Kim, E. M. Renz, D. Barillo, J. B. Holcomb, C. E. Wade, and S. E. Wolf, "Contribution of bacterial and viral infections to attributable mortality in patients with severe burns: An autopsy series," Burns **36**(6), 773–779 (2010).
[3]R. L. Bang, P. N. Sharma, S. C. Sanyal, and I. Al Najjadah, "Septicaemia after burn injury: A comparative study," Burns **28**(8), 746–751 (2002).
[4]J. A. Fishman and R. H. Rubin, "Infection in organ-transplant recipients," N. Engl. J. Med. **338**(24), 1741–1751 (1998).
[5]J. S. Dummer, C. G. Montero, B. P. Griffith, R. L. Hardesty, I. L. Paradis, and M. Ho, "Infections in heart-lung transplant recipients," Transplantation **41**(6), 725–729 (1986).
[6]G. B. Pier, "Pulmonary disease associated with *Pseudomonas aeruginosa* in cystic fibrosis: Current status of the host-bacterium interaction," J. Infect. Dis. **151**(4), 575–580 (1985).
[7]F. Marchetti, L. Giglio, M. Candusso, D. Faraguna, and B. Assael, "Early antibiotic treatment of *Pseudomonas aeruginosa* colonisation in cystic fibrosis: A critical review of the literature," Eur. J. Clin. Pharmacol. **60**(2), 67–74 (2004).
[8]G. Maschmeyer and I. Braveny, "Review of the incidence and prognosis of *Pseudomonas aeruginosa* infections in cancer patients in the 1990s," Eur. J. Clin. Microbiol. Infect. Dis. **19**(12), 915–925 (2000).
[9]R. Manfredi, A. Nanetti, M. Ferri, and F. Chiodo, "Pseudomonas spp. complications in patients with HIV disease: An eight-year clinical and microbiological survey," Eur. J. Epidemiol. **16**(2), 111–118 (2000).
[10]J. W. Costerton, P. S. Stewart, and E. P. Greenberg, "Bacterial biofilms: A common cause of persistent infections," Science **284**, 1318 (1999).
[11]H. B. Sheth, K. K. Lee, W. Y. Wong, G. Srivastava, O. Hindsgaul, R. S. Hodges, W. Paranchych, and R. T. Irvin, "The pili of *Pseudomonas aeruginosa* strains PAK and PAO bind specifically to the carbohydrate sequence βGalNAc(1–4)βGal found in glycosphingolipids asialo-GM1 and asialo-GM2," Mol. Microbiol. **11**(4), 715–723 (1994).
[12]K. K. Lee, H. B. Sheth, W. Y. Wong, R. Sherburne, W. Paranchych, R. S. Hodges, C. A. Lingwood, H. Krivan, and R. T. Irvin, "The binding of *Pseudomonas aeruginosa* pili to glycosphingolipids is a tip-associated event involving the C-terminal region of the structural pilin subunit," Mol. Microbiol. **11**(4), 705–713 (1994).
[13]L. L. Burrows, "Weapons of mass retraction," Mol. Microbiol. **57**(4), 878–888 (2005).
[14]L. L. Burrows, "*Pseudomonas aeruginosa* twitching motility: Type IV pili in action," Annu. Rev. Microbiol. **66**(1), 493–520 (2012).
[15]L. Craig, M. E. Pique, and J. A. Tainer, "Type IV pilus structure and bacterial pathogenicity," Nat. Rev. Microbiol. **2**(5), 363–378 (2004).
[16]J. S. Mattick, "Type IV pili and twitching motility," Annu. Rev. Microbiol. **56**(1), 289–314 (2002).
[17]F. Jin, J. C. Conrad, M. L. Gibiansky, and G. C. L. Wong, "Bacteria use type-IV pili to slingshot on surfaces," Proc. Natl. Acad. Sci. U.S.A. **108**(31), 12617–12622 (2011).
[18]J. C. Conrad, M. L. Gibiansky, F. Jin, V. D. Gordon, D. A. Motto, M. A. Mathewson, W. G. Stopka, D. C. Zelasko, J. D. Shrout, and G. C. L. Wong, "Flagella and pili-mediated near-surface single-cell motility mechanisms in *P. aeruginosa*," Biophys. J. **100**(7), 1608–1616 (2011).
[19]J. M. Skerker and H. C. Berg, "Direct observation of extension and retraction of type IV pili," Proc. Natl. Acad. Sci. U.S.A. **98**(12), 6901–6904 (2001).
[20]G. O'Toole, H. B. Kaplan, and R. Kolter, "Biofilm formation as microbial development," Annu. Rev. Microbiol. **54**(1), 49–79 (2000).
[21]K. B. Barken, S. J. Pamp, L. Yang, M. Gjermansen, J. J. Bertrand, M. Klausen, M. Givskov, C. B. Whitchurch, J. N. Engel, and T. Tolker-Nielsen, "Roles of type IV pili, flagellum-mediated motility and extracellular DNA in the formation of mature multicellular structures in *Pseudomonas aeruginosa* biofilms," Environ. Microbiol. **10**(9), 2331–2343 (2008).
[22]M. Allesen-Holm, K. B. Barken, L. Yang, M. Klausen, J. S. Webb, S. Kjelleberg, S. Molin, M. Givskov, and T. Tolker-Nielsen, "A characterization of DNA release in *Pseudomonas aeruginosa* cultures and biofilms," Mol. Microbiol. **59**(4), 1114–1128 (2006).

[23]H. Mikkelsen, M. Sivaneson, and A. Filloux, "Key two-component regulatory systems that control biofilm formation in *Pseudomonas aeruginosa*," Environ. Microbiol. **13**(7), 1666–1681 (2011).
[24]S. N. Abraham, A. B. Jonsson, and S. Normark, "Fimbriae-mediated host-pathogen cross-talk," Curr. Opin. Microbiol. **1**(1), 75–81 (1998).
[25]D. Dubnau, "DNA Uptake in Bacteria," Annu. Rev. Microbiol. **53**(1), 217–244 (1999).
[26]E. J. van Schaik, C. L. Giltner, G. F. Audette, D. W. Keizer, D. L. Bautista, C. M. Slupsky, B. D. Sykes, and R. T. Irvin, "DNA binding: A novel function of *Pseudomonas aeruginosa* type IV pili," J. Bacteriol. **187**(4), 1455–1464 (2005).
[27]D. Bieber, S. W. Ramer, C. Y. Wu, W. J. Murray, T. Tobe, R. Fernandez, and G. K. Schoolnik, "Type IV pili, transient bacterial aggregates, and virulence of enteropathogenic Escherichia coli," Science **280**(5372), 2114–2118 (1998).
[28]D. A. Herrington, R. H. Hall, G. Losonsky, J. J. Mekalanos, R. K. Taylor, and M. M. Levine, "Toxin, toxin-coregulated pili, and the toxR regulon are essential for Vibrio cholerae pathogenesis in humans," J. Exp. Med. **168**(4), 1487–1492 (1988).
[29]H. E. Parge, K. T. Forest, M. J. Hickey, D. A. Christensen, E. D. Getzoff, and J. A. Tainer, "Structure of the fibre-forming protein pilin at 2.6 A resolution," Nature **378**(6552), 32–38 (1995).
[30]B. Hazes, P. A. Sastry, K. Hayakawa, R. J. Read, and R. T. Irvin, "Crystal structure of *Pseudomonas aeruginosa* PAK pilin suggests a main-chain-dominated mode of receptor binding," J. Mol. Biol. **299**(4), 1005–1017 (2000).
[31]D. W. Keizer, C. M. Slupsky, M. Kalisiak, A. P. Campbell, M. P. Crump, P. A. Sastry, B. Hazes, R. T. Irvin, and B. D. Sykes, "Structure of a pilin monomer from *Pseudomonas aeruginosa*: Implications for the assembly of pili," J. Biol. Chem. **276**(26), 24186–24193 (2001).
[32]G. F. Audette, R. T. Irvin, and B. Hazes, "Crystallographic analysis of the *Pseudomonas aeruginosa* strain K122-4 monomeric pilin reveals a conserved receptor-binding architecture," Biochemistry **43**(36), 11427–11435 (2004).
[33]D. J. Kao, M. E. A. Churchill, R. T. Irvin, and R. S. Hodges, "Animal protection and structural studies of a consensus sequence vaccine targeting the receptor binding domain of the type IV pilus of *Pseudomonas aeruginosa*," J. Mol. Biol. **374**(2), 426–442 (2007).
[34]Y. Nguyen, S. G. Jackson, F. Aidoo, M. Junop, and L. L. Burrows, "Structural characterization of novel *Pseudomonas aeruginosa* type IV pilins," J. Mol. Biol. **395**(3), 491–503 (2010).
[35]S. Hartung, A. S. Arvai, T. Wood, S. Kolappan, D. S. Shin, L. Craig, and J. A. Tainer, "Ultrahigh resolution and full-length pilin structures with insights for filament assembly, pathogenic functions, and vaccine potential," J. Biol. Chem. **286**(51), 44254–44265 (2011).
[36]J. Li, E. H. Egelman, and L. Craig, "Structure of the vibrio cholerae type IVb pilus and stability comparison with the *Neisseria gonorrhoeae* type IVa pilus," J. Mol. Biol. **418**(1–2), 47–64 (2012).
[37]L. Craig, R. K. Taylor, M. E. Pique, B. D. Adair, A. S. Arvai, M. Singh, S. J. Lloyd, D. S. Shin, E. D. Getzoff, M. Yeager, K. T. Forest, and J. A. Tainer, "Type IV pilin structure and assembly: X-ray and EM analyses of vibrio cholerae toxin-coregulated pilus and *Pseudomonas aeruginosa* PAK pilin," Mol. Cell **11**(5), 1139–1150 (2003).
[38]K. H. Piepenbrink, G. A. Maldarelli, C. F. M. de la Peña, G. L. Mulvey, A. Lee, E. C. von Rosenvinge, G. D. Armstrong, M. S. Donnenberg, and E. J. Sundberg, "Structural and evolutionary analyses show unique stabilization strategies in the type IV Pili of *Clostridium difficile*," Structure **23**(2), 385–396 (2015).
[39]V. Pelicic, "Type IV pili: e pluribus unum?," Mol. Microbiol. **68**(4), 827–837 (2008).
[40]K. T. Forest and J. A. Tainer, "Type-4 pilus-structure: Outside to inside and top to bottom—minireview," Gene **192**(1), 165–169 (1997).
[41]L. Craig and J. Li, "Type IV pili: Paradoxes in form and function," Curr. Opin. Struct. Biol. **18**(2), 267–277 (2008).
[42]B. Hazes and L. Frost, "Towards a systems biology approach to study type II/IV secretion systems," Biochim. Biophys. Acta– Biomembr. **1778**(9), 1839–1850 (2008).
[43]M. Ayers, P. L. Howell, and L. L. Burrows, "Architecture of the type II secretion and type IV pilus machineries," Future Microbiol. **5**(8), 1203–1218 (2010).
[44]L. Craig, N. Volkmann, A. S. Arvai, M. E. Pique, M. Yeager, E. H. Egelman, and J. A. Tainer, "Type IV pilus structure by cryo-electron microscopy and crystallography: Implications for pilus assembly and functions," Mol. Cell **23**(5), 651–662 (2006).
[45]W. Folkhard, D. A. Marvin, T. H. Watts, and W. Paranchych, "Structure of polar pili from *Pseudomonas aeruginosa* strains K and O," J. Mol. Biol. **149**(1), 79–93 (1981).
[46]B. Maier, L. Potter, M. So, H. S. Seifert, and M. P. Sheetz, "Single pilus motor forces exceed 100 pN," Proc. Natl. Acad. Sci. U.S.A. **99**(25), 16012–16017 (2002).
[47]C. L. Giltner, E. J. van Schaik, G. F. Audette, D. Kao, R. S. Hodges, D. J. Hassett, and R. T. Irvin, "The *Pseudomonas aeruginosa* type IV pilin receptor binding domain functions as an adhesin for both biotic and abiotic surfaces," Mol. Microbiol. **60**(3), 813–813 (2006).
[48]B. Yu, C. L. Giltner, E. J. Van Schaik, D. L. Bautista, R. S. Hodges, G. F. Audette, D. Y. Li, and R. T. Irvin, "A novel biometallic interface: High affinity tip-associated binding by pilin-derived protein nanotubes," J. Bionanosci. **1**(2), 73–83 (2007).
[49]G. Reguera, K. D. McCarthy, T. Mehta, J. S. Nicoll, M. T. Tuominen, and D. R. Lovley, "Extracellular electron transfer via microbial nanowires," Nature **435**(7045), 1098–1101 (2005).
[50]H. Yi, K. P. Nevin, B. C. Kim, A. E. Franks, A. Klimes, L. M. Tender, and D. R. Lovley, "Selection of a variant of Geobacter sulfurreducens with enhanced capacity for current production in microbial fuel cells," Biosens. Bioelectron. **24**(12), 3498–3503 (2009).
[51]N. S. Malvankar, M. Vargas, K. P. Nevin, A. E. Franks, C. Leang, B.-C. Kim, K. Inoue, T. Mester, S. F. Covalla, J. P. Johnson, V. M. Rotello, M. T. Tuominen, and D. R. Lovley, "Tunable metallic-like conductivity in microbial nanowire networks," Nat. Nanotechnol. **6**(9), 573–579 (2011).
[52]N. S. Malvankar, T. Mester, M. T. Tuominen, and D. R. Lovley, "Supercapacitors based on c-type cytochromes using conductive nanostructured networks of living bacteria," ChemPhysChem **13**(2), 463–468 (2012).
[53]G. F. Audette, E. J. vanSchaik, B. Hazes, and R. T. Irvin, "DNA-binding protein nanotubes: Learning from nature's nanotech examples," Nano Lett. **4**(10), 1897–1902 (2004).
[54]S. Lombardo, S. Z. Jasbi, S.-K. Jeung, S. Morin, and G. F. Audette, "Initial studies of protein nanotube oligomerization from a modified gold surface," J. Bionanosci. **3**(1), 61–65 (2009).

[55]A. Petrov, S. Lombardo, and G. Audette, "Fibril–mediated oligomerization of pilin-derived protein nanotubes," J. Nanobiotechnol. **11**(1), 24 (2013).
[56]T. Rob and D. J. Wilson, "Time-resolved mass spectrometry for monitoring millisecond time-scale solution-phase processes," Eur. J. Mass Spectrom. **18**(2), 205–214 (2012).
[57]L. Konermann, J. Pan, and D. J. Wilson, "Protein folding mechanisms studied by time-resolved electrospray mass spectrometry," BioTechniques **40**(2), 135, 137, 139 passim (2006).
[58]A. J. Percy, M. Rey, K. M. Burns, and D. C. Schriemer, "Probing protein interactions with hydrogen/deuterium exchange and mass spectrometry-a review," Anal. Chim. Acta **721**, 7–21 (2012).
[59]H. C. Neu and L. A. Heppel, "The release of enzymes from *Escherichia coli* by osmotic shock and during the formation of spheroplasts," J. Biol. Chem. **240**(9), 3685–3692 (1965).
[60]T. Rob, P. Liuni, P. K. Gill, S. Zhu, N. Balachandran, P. J. Berti, and D. J. Wilson, "Measuring dynamics in weakly structured regions of proteins using microfluidics-enabled subsecond H/D exchange mass spectrometry," Anal Chem. **84**(8), 3771–3779 (2012).
[61]Y.-Z. Zhang, Ph.D., University of Pennsylvania, 1995.
[62]J.-Y. Suh, L. Spyracopoulos, D. W. Keizer, R. T. Irvin, and B. D. Sykes, "Backbone dynamics of receptor binding and antigenic regions of a *Pseudomonas aeruginosa* pilin monomer," Biochemistry **40**(13), 3985–3995 (2001).
[63]The PyMOL Molecular Graphics System, Version 1.7.4, Schrodinger, LLC.